Shallow trap states in pentacene thin films from molecular sliding

Joo H. Kang, Demetrio da Silva Filho, Jean-Luc Bredas, and X.-Y. Zhu

Citation: Appl. Phys. Lett. **86**, 152115 (2005); doi: 10.1063/1.1900944
View online: http://dx.doi.org/10.1063/1.1900944
View Table of Contents: http://apl.aip.org/resource/1/APPLAB/v86/i15
Published by the American Institute of Physics.

Shallow trap states in pentacene thin films from molecular sliding

Joo H. Kang
Department of Chemistry, University of Minnesota, Minneapolis, Minnesota 55455

Demetrio da Silva Filho and Jean-Luc Bredas
School of Chemistry and Biochemistry, Georgia Institute of Technology, Atlanta, Georgia 30332

X.-Y. Zhu[a)]
Department of Chemistry, University of Minnesota, Minneapolis, Minnesota 55455

(Received 13 December 2004; accepted 1 March 2005; published online 8 April 2005)

Petacene is one of the most promising organic semiconductors for thin-film transistors. Transport measurements in the past have established the presence of shallow traps but their origins have remained a mystery. Here we show that shallow traps in vapor-deposited crystalline pentacene thin films are due to local defects resulting from the sliding of pentacene molecules along their long molecular axis, while two-dimensional crystalline packing is maintained. Electronic structural calculation confirms that these sliding defects are shallow-charge traps with energies $\leqslant 100$ meV above (below) the valence band maximum (conduction band minimum). © *2005 American Institute of Physics*. [DOI: 10.1063/1.1900944]

Organic thin-film transistors[1] (OTFTs) are key components in molecule-based electronics and optoelectronics. Among the most promising organic semiconductors is pentacene, which has shown the highest carrier mobility[2–5] in OTFTs. Since charge transport in OTFT occurs within the first few layers of molecules in contact with the dielectric,[6] we must understand the structure–property relationship in the interface region. While a judicious choice of deposition conditions has dramatically decreased domain boundary densities,[7] and thus deep traps in vapor-deposited pentacene thin films, little is known about the nature of shallow trap states observed in transport measurements.[2,8] Here we show the origin of shallow trap states using molecular resolution imaging and electronic–structure calculations. These shallow traps are formed from the sliding of pentacene molecules along their long molecular axis while two-dimensional crystallinity is maintained.

Pentacene is a prototypical van der Waals organic solid[9,10] consisting of stacked layers of molecules with interplane spacing $d_{001}=14.1$ Å. Within each layer (the *ab* plane), the molecules are arranged in a herringbone motif. The structure of pentacene thin films deposited on various solid substrates has been extensively studied. When interaction with the solid substrate is weak (e.g., on oxide or molecular monolayer passivated surfaces), pentacene molecules nucleate to form the "standing-up," bulklike crystalline layers with the *ab* plane parallel to the substrate. The interplane spacing in the thin-film phase is usually larger than that of bulk pentacene: $d_{001}=14.1$–16.1 Å,[10–13] attributed to different tilting angles of the long molecular axis. When interaction with the solid surface is strong, pentacene molecules adsorb in a "lying-down" geometry.[14–17]

An ideal approach to probe local defects is real–space imaging. For the standing-up phase of pentacene, only low-resolution imaging of crystalline domain size, shape, and height has been possible in the past by atomic force microscopy,[13] photoelectron emission microscopy[7] (PEEM), and scanning tunneling microscopy (STM).[18] Here we demonstrate that local defects in standing-up pentacene thin films can be visualized by STM with high impedance. We choose Au(111) because of the ease with which a passivation layer, benzenethiol (BT) self-assembled monolayer (SAM), can be formed on the surface for the growth of the standing-up pentacene phase (see cartoon in Fig. 1). In a similar approach, Halik *et al.* demonstrated a high-mobility and low-voltage OTFT from pentacene thin films vapor deposited on a phenyl-terminated SAM.[5]

Clean Au(111) was prepared in ultrahigh vacuum (UHV) using sputtering–annealing procedures and verified by STM. A SAM was formed by exposing Au(111) to $\geqslant 10^3$ Lang-

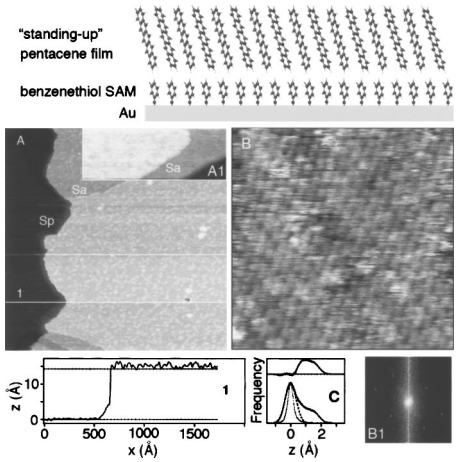

FIG. 1. Pentacene monolayer deposited at 295 K on BT–SAM/Au(111). Panel A (2435 Å × 2435 Å): regions of both BT–SAM (left) and pentacene monolayer (right). Inset A1: (602 Å × 248 Å): BT–SAM region. *Sa* = Step of Au(111); *Sp* = Step of the pentacene layer. Panel B (100 Å × 100 Å): pentacene monolayer. Panel B1: Fourier transform from the monolayer image of a larger area. Panel 1: line section from A. Panel C: height histograms of the pentacene monolayer (thick solid curve) and BT–SAM (thin solid curve). The latter can be fitted with a Gaussian with full width at half maximum (FWHM) = 0.54 ± 0.05 Å. The dashed curve is a Gaussian fit (FWHM = 0.95 ± 0.06 Å) to the main component in the thick solid curve. The upper curve is the difference between the thick solid and the dashed curves.

[a)]Author to whom correspondence should be addressed; electronic mail: zhu@chem.umn.edu

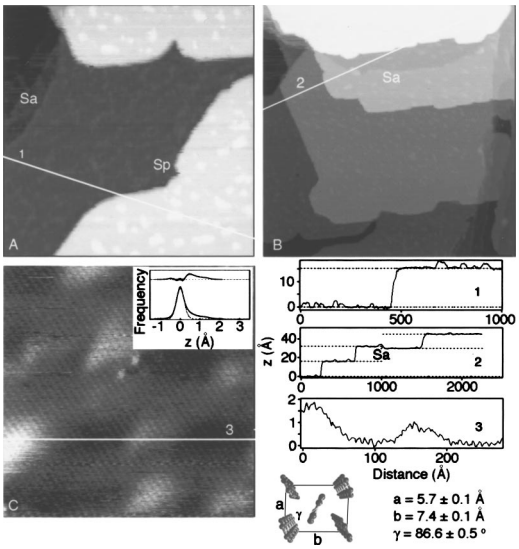

FIG. 2. Multilayer pentacene films vapor deposited on BT–SAM-covered Au(111) at 295 K. Panel A (970 Å×970 Å) shows a region consisting of both monolayer and bilayer pentacene. Panel B (2490 Å×2490 Å) shows a region with up to 5 layers of pentacene. Panel C (280 Å×280 Å) shows a zoom-in image of a pentacene multilayer. The inset in C shows a height histogram of the multilayer. The dashed curve is a Gaussian fit (FWHM $=0.55\pm0.05$ Å) to the main component and the upper curve is the difference. Three line sections (1–3) are also shown.

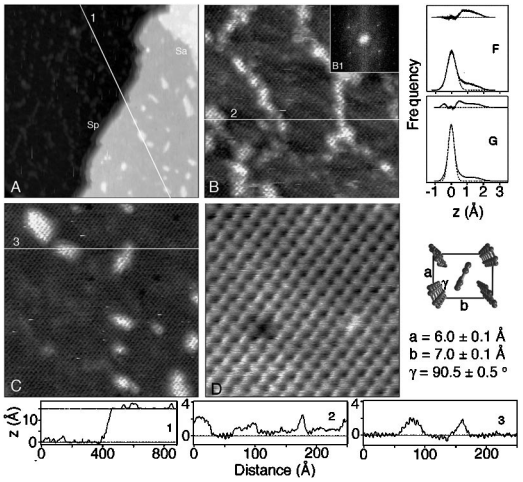

FIG. 3. STM images of ~2 ML pentacene vapor deposited on BT–SAM-covered Au(111) at 333 K. Panel A (800 Å×800 Å) shows a region consisting of both monolayer and bilayer pentacene. Panel B (250 Å×250 Å) shows the zoom in of the monolayer region, with a Fourier transform in B1. Panel C (250 Å×250 Å) shows the zoom-in of the second layer. Panel D (65 Å×65 Å) shows the molecular resolution image of a relatively flat region on the second layer. Three line sections (1–3) are also shown, along with height histograms of the first (F) and second layer (G). On each histogram, the dashed curve is a Gaussian fit (FWHM $=0.83\pm0.3$ Å for F and 0.55 ± 0.2 Å for G) to the main component and the upper curve is the difference.

muirs of benzenethiol (BT) at 295 K. Pentacene was vapor deposited onto the BT–SAM/Au(111) surface at substrate temperatures of 295 and 333 K from a Knudsen cell. The deposition rate was 1.4 ± 0.1 Å/min as monitored by a quartz–crystal microbalance. Before deposition, pentacene was outgassed at 423 K overnight in UHV. A film thickness of 15 Å was defined as one monolayer (ML). Images were taken using an UHV–STM (RHK) at room temperature in a constant current mode with an impedance of 10-100 GW.

Panel A in Fig. 1 shows the STM image of 0.7 ML pentacene deposited on BT–SAM at 295 K. Regions of the pentacene monolayer and the BT–SAM are distinguishable morphologically. The former contains a large number of protruding defects, while the latter is much smoother (A1). Line section (1) across the boundary shows a step height of $d_{001}=14.2\pm0.1$ Å, corresponding to the standing-up phase. The histogram of the pentacene monolayer (panel C) is characterized by a main Gaussian component and a positive tail (protruding defects) accounting for 36 ± 5 % of the surface area with an average height of $\langle h+\rangle=1.2\pm0.1$ Å. For comparison, the histogram of the BT–SAM surface shows a much narrower distribution. Zooming in on the monolayer (panel B) reveals the lattice resolution. The two-dimensional (2D) Fourier transform gives in-plane lattice parameters of $a=5.7\pm0.1$ Å, $b=7.4\pm0.1$ Å, and $\gamma=86.6°\pm0.5°$. The area of the unit cell is smaller than that of bulk pentacene in the *ab* plane,[9,10] in agreement with previous studies on thin films.[10–13]

Figure 2 shows images obtained for ~2 ML pentacene. The pentacene film does not grow layer by layer, as we find regions where the monolayer and the bilayer coexist (panel A), as well as regions covered with a maximum of 5 ML (panel B). Line sections (1) and (2) show that the step height for each pentacene layer is $d_{100}=15.1\pm0.2$ Å (terrace to terrace) for all film thickness above 1 ML. The height distribution (E) is characterized by a main Gaussian component and a positive tail (22%) with $\langle h+\rangle=0.8\pm0.1$ Å. There is also a small percentage (3%) on the negative side, with an average depth of $\langle h-\rangle=-0.5\pm0.1$ Å. We found no quantitative differences for 2–5 ML.

A zoom-in image (C) and its line section (3) reveals details of the protruding defects: (i) There is a broad distribution in the heights, ranging from a fraction of 1 to ~2 Å; (ii) each defect island merges smoothly into the surrounding; (iii) the 2D lattice is *not* affected by the defects. Fourier analysis gives 2D lattice parameters identical to those in the monolayer. Because the 2D lattice is maintained throughout each crystalline domain, including defect islands, these defects must come from the sliding of pentacene molecules along their long axis, while herringbone packing in the *ab* plane is maintained. We argue that the formation of these defects is intrinsic to the growth of each pentacene layer because the morphology of the second layer is distinctively different from and does not reflect the morphology of the first pentacene layer. The defect islands are immobile at room temperature, but reorganize upon annealing at 353 K to give more regular shaped islands with the boundary oriented preferentially along [10] and [11] directions in the *ab* plane.

Substrate temperature during deposition affects defect distribution. Figure 3 shows images for ~2 ML pentacene deposited at 333 K when growth is mainly layer by layer. Panel A shows a region consisting both 1 and 2 ML. A line section (1) shows a step height of $d_{001}=15.1\pm0.1$ Å for the second layer. Panel B shows a zoom-in image of the first layer. The 2D crystalline lattice is visible throughout the image, including all islands. The Fourier transform of the image (B1) gives a nearly rectangular lattice. A histogram height analysis of the monolayer image (panel F) shows bimodal distribution, a main Gaussian component, and a positive tail (21 ± 2 %) with $\langle h+\rangle=1.2\pm0.1$ Å. Compared to that at 295 K, growth at 333 K gives a smoother film.

A representative region of the second layer is shown in panel C. The 2D lattice runs through all defect islands. The

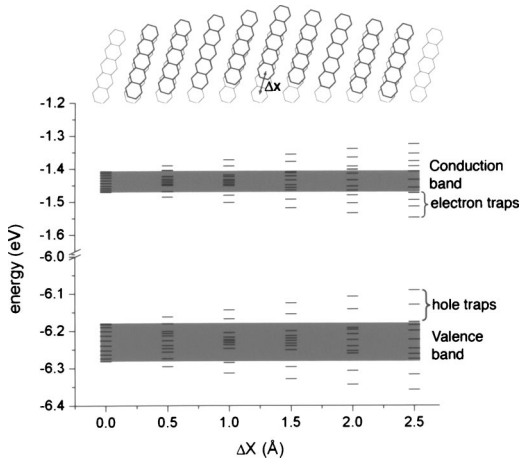

FIG. 4. Top: Illustration of the defect considered in the INDO calculations. Here, the grey molecules are stacked along the *a* direction and the darker molecules model the kinds of stacks within a structural defect. The data shows evolution of molecular orbitals within the structural defect for a stack along *a*, as a function of the maximum displacement Δx along the long molecular axis.

molecular resolution image (D) of the relatively flat terrace clearly shows the herringbone packing. The fourier transform of images from 2 ML gives the same lattice parameters as those for the 1 ML. A histogram height analysis (G) of the second layer shows a main Gaussian component, a positive tail $(21\pm2\ \%)$ with $\langle h+\rangle=1.2\pm0.1$ Å, and a small negative tail $(4\pm1\ \%)$ with $\langle h-\rangle=-0.5\pm0.1$ Å. Change in deposition temperature also leads to a change in unit cell dimension, but not in 2D unit cell area.

A major issue raised by the STM results is whether these sliding defects induce shallow trap states for carrier transport. To answer this question, we performed a series of quantum–chemical calculations. In particular, we were interested in evaluating the evolution of the HOMO and LUMO (highest occupied and lowest unoccupied molecular orbitals) energies when considering the defect structures. In order to allow an easy comparison with our previous studies on defect-free pentacene,[19,20] we used the semiempirical intermediate neglect of differential overlap (INDO) method.[21,22] As early studies on pentacene crystals have demonstrated,[19,20,23] significant electronic couplings are found only within the herringbone *ab* planes, especially along the *a* axis and along the so-called diagonal axes (d_1 and d_2).[19,24] Here, we considered stacks made of 11 molecules either along the *a* direction or the d_1 diagonal direction. The molecules were initially positioned at their locations in the single crystal structure[13] (zero displacement); they were then displaced along their long molecular axis as illustrated in Fig. 4 to model the structure seen in the defects. For zero displacement, the dispersions of the highest occupied molecular orbitals (HOMOs) and lowest unoccupied molecular orbitals (LUMOs) were used to define the defect-free conduction and valence bands. For molecules stacked along the *a* direction (the results are similar for the d_1 direction), it is seen that the defect induces the appearance of *both hole and electron levels in the gap*. For the maximum displacement Δx of 2.5 Å that corresponds to the experimental observations, the HOMO and LUMO levels in the defect are removed by ~100 meV from the corresponding levels in the absence of defects. Thus, the height distribution seen in the defect islands corresponds to shallow traps for both positive and negative carriers, with energies in the range of 0–100 meV. For comparison, experimentally determined activation energy in transport measurements is ~30 meV for films grown at room temperature.[8] Higher activation energies have been observed for films grown above room temperature.[25] Our STM results explain this observation: Compared to that at 295 K, the histogram of 2 ML grown at 333 K shows a reduction in the number of shorter islands but an increase in that of taller islands and, thus, deeper traps.

We note that the reason why the valence and conduction bandwidths increase with displacement is to be found in the details of the HOMO and LUMO wave function overlaps between adjacent molecules[20] and their evolution with displacement. We emphasize that, depending on the initial relative positions of adjacent molecules, a displacement along the long molecular axis can either increase or reduce the bandwidths.[20] Thus, obtaining a microscopic knowledge of structural defects is key to understanding the extent of their impact on electronic structure and carrier dynamics.

This work was supported by the National Science Foundation through Grant No. DMR 0238307 and by the MRSEC Program under Award No. DMR-0212302.

[1] G. Horowitz, Adv. Mater. (Weinheim, Ger.) **10**, 365 (1998).
[2] S. F. Nelson, Y.-Y. Lin, D. J. Gundlach, and T. N. Jackson, Appl. Phys. Lett. **72**, 1854 (1998).
[3] M Shtein, J. Mapel, J. B. Benziger, and S. R. Forrest, Appl. Phys. Lett. **81**, 268 (2002).
[4] T. Minari, T. Nemoto, and S. Isoda, J. Appl. Phys. **96**, 769 (2004).
[5] M. Halik *et al.*, Nature (London) **431**, 963 (2004).
[6] A. Dodabalapur, L. Torsi, and H. E. Katz, Science **268**, 270 (1995).
[7] F.-J. Meyer zu Heringdorf, M. C. Reuter, and R. M. Tromp, Nature (London) **412**, 517 (2001).
[8] P. V. Pesavento, R. J. Chesterfield, C. R. Newman, and C. D. Frisbie, J. Appl. Phys. **96**, 7312 (2004).
[9] T. Siegrist *et al.*, Angew. Chem., Int. Ed. **40**, 1732 (2001).
[10] C. C. Mattheus *et al.*, Acta Crystallogr., Sect. C: Cryst. Struct. Commun. **C57**, 939 (2001).
[11] T. Minakata, H. Imai, M. Ozaki, and K. Saco, J. Appl. Phys. **72**, 5220 (1992).
[12] C. C. Mattheus *et al.*, Synth. Met. **138**, 475 (2003).
[13] S. E. Fritz, S. M. Martin, C. D. Frisbie, M. D. Ward, and M. F. Toney, J. Am. Chem. Soc. **126**, 4084 (2004).
[14] C. B. France, P. G. Schroeder, and B. A. Parkinson, Nano Lett. **2**, 693 (2002).
[15] S. Lukas, G. Witte, and Ch. Wöll, Phys. Rev. Lett. **88**, 028301 (2002).
[16] J. H. Kang and X.-Y. Zhu, Appl. Phys. Lett. **82**, 3248 (2003).
[17] Y. L. Wang, W. Ji, D. X. Shi, S. X. Du, C. Seidel, Y. G. Ma, H.-J. Gao, L. F. Chi, and H. Fuchs, Phys. Rev. B **69**, 075408 (2004).
[18] D. Fichou, F. Charra, and A. O. Gusev, Adv. Mater. (Weinheim, Ger.) **13**, 555 (2001).
[19] J. Cornil, J. P. Calbert, and J. L. Bredas, J. Am. Chem. Soc. **123**, 1250 (2001).
[20] J. L. Bredas, J. P. Calbert, D. A. Da Silva Filho, and J. Cornil, Proc. Natl. Acad. Sci. U.S.A. **99**, 5804 (2002).
[21] J. Ridley and M. Zerner, Theor. Chim. Acta **32**, 111 (1973).
[22] M. C. Zerner, G. H. Loew, R. F. Kirchner, and U. T. Mueller-Westerhoff, J. Am. Chem. Soc. **102**, 589 (1980).
[23] G. A. de Wijs, C. C. Mattheus, R. A. de Groot, and T. T. M. Palstra, Synth. Met. **139**, 109 (2003).
[24] Y. C. Cheng, R. J. Silbey, D. A. da Silva Filho, J. P. Calbert, J. Cornil, and J. L. Bredas, J. Chem. Phys. **118**, 3764 (2003).
[25] J. Lee, J. H. Kim, and S. Im, J. Appl. Phys. **95**, 3733 (2004).